



## **Edge Detection and Depth to Magnetic Source Estimation in Part of Central Nigeria**

**Mam D. Tawey<sup>1\*</sup>, Abbass A. Adetona<sup>2</sup>, Usman D. Alhassan<sup>2</sup>,  
Abdulwaheed A. Rafiu<sup>2</sup>, Kazeem A. Salako<sup>2</sup> and Emmanuel E. Udensi<sup>2</sup>**

<sup>1</sup>*National Water Resources Institute, Mando Road, Kaduna, Nigeria.*

<sup>2</sup>*Geophysics Department, Federal University of Technology, Minna, Nigeria.*

### **Authors' contributions**

*This work was carried out in collaboration among all authors. Author MDT designed the study, performed the statistical analysis, wrote the protocol and wrote the first draft of the manuscript. Authors AAA and UDA managed the analyses of the study. Authors AAR, KAS and EEU managed the literature searches. All authors read and approved the final manuscript.*

### **Article Information**

DOI: 10.9734/PSIJ/2020/v24i730203

#### Editor(s):

(1) Dr. Lei Zhang, Winston-Salem State University, USA.

(2) Dr. Thomas F. George, University of Missouri, USA.

#### Reviewers:

(1) Muralitharan Jothimani, University of Gondar, Ethiopia.

(2) Alemu Gurmessa Gindaba, Wollega University, Ethiopia.

Complete Peer review History: <http://www.sdiarticle4.com/review-history/60263>

**Original Research Article**

**Received 22 June 2020**  
**Accepted 27 August 2020**  
**Published 09 September 2020**

### **ABSTRACT**

High-resolution aeromagnetic data covering an area of 24, 200 km<sup>2</sup> in north central Nigeria has been acquired and analyzed with the aim of carrying out trend analysis, edge detection (structural delineation) and depth to magnetic source estimation using reduce to the pole (RTP), horizontal gradient magnitude (HGM), center for exploration targeting plug-in (CET), 3D Euler deconvolution and source parameter imaging (SPI) techniques. Trend analysis was applied to the RTP data to delineate structures that have dissected the area. The 3D Euler deconvolution and HGM were correlated by plotting the estimated Euler solutions for a structural index of one (SI=1) on HGM map and the resulting map produced have shown that both methods can contribute in the interpretation of the general structural framework of the study area. The structural delineation based on HGM and CET maps showed that two predominant trends (ENE-WSW) and (WNW-ENE) have affected the area. The trend/depth/contacts of these faults were classified into four groups: Faults <150 m, 150 m - 300 m, 300m - 450 m which are the most predominant fault system based on Euler solutions with a structural index of one (SI=1) and those deeper than 450 m while the result of source parameter imaging (SPI) revealed a depth to source varying from 58 m specifically

\*Corresponding author: E-mail: [taweymam@gmail.com](mailto:taweymam@gmail.com);

for areas with shallow depth to the magnetic source to those from deeper source occurring at 588.153m depth especially the south-central portion and the south-eastern portion of the study area.

*Keywords: RTP; HGM; CET; deconvolution; SPI.*

## 1. INTRODUCTION

Magnetic surveying has broad range of applications, from small scale engineering or archaeological surveys to detect buried metallic objects, to large-scale surveys carried out to investigate the regional geological structure. Common causes of magnetic anomalies include dykes, faulted, folded or truncated sills and lava flows, massive basic intrusions, metamorphic basement rocks and magnetite ore bodies [1]. The magnetic method has been widely used in mineral exploration for decades, recent improvements in magnetic data acquisition, processing and presentation have increased the importance of magnetic surveys; particularly the high-resolution aeromagnetic surveys[2]. In High-resolution aeromagnetic data (HRAD), the data are generally collected as close to the ground as allowed by aircraft safety and regulations, giving nominal terrain clearances of about 80-150 m [3]. This great advance to aeromagnetic interpretation has been a change in the survey design that better map short wavelength, low-amplitude magnetic anomalies[4]and is a time and cost-effective method of mapping the Earth's magnetic field. Magnetic anomalies in the Earth magnetic field are caused by magnetic minerals in the rocks, and maps and images of these anomalies can be interpreted in terms of geology. The modern aeromagnetic survey is capable of mapping valuable geologic structures on a regional scale including concealed terrains due to the sophistication of modern technology to provide high-quality data [5 – 7] . Airborne geophysical data can be enhanced by a range of linear and non-linear filtering algorithms. A range of imaging routines can be specified to visually enhance the effects of selected geologic sources using mathematical enhancement techniques[8]. The interpretation of aeromagnetic anomaly data for improved sources depth estimates and locations of structural features such as faults, folds and contacts requires the use of relevant standard techniques and good geological interpretation. Some of these standard techniques include: A transformation operation launched by [9] and developed by [10] called Pole Reduction (RTP) that enables the repositioning of magnetic anomalies above the

causative source, horizontal gradient magnitude (HGM) technique that can be used to map linear features [11 – 13], such as fault zones and/or dykes from the potential field data compared with the application of center for exploration targeting (CET) for automatic structural delineation which according to [14, 15], is a suite of algorithms that provide enhancement, lineament detection and Structural complexity analysis functionalities for potential field data with Euler deconvolution [16], for a boarder, structures, depth and geometry as well as source parameter imaging developed by [17 – 19] for depth to magnetic source determination as such, the present research is aimed at the delineation of structural framework and depth to the magnetic source within the study area and we applied the above-mentioned transformation and filtering techniques to delineate these structures and depth to the magnetic source within part of north-central Nigeria bearing in mind, the association of structures with mineralization. Several articles have been published based on interpretation of aeromagnetic data within Nigerian basement complex and adjoining sedimentary basins[20 – 25] which some of the techniques mentioned above were used.

### 1.1 Location of the Study Area

The research area is a rectangular block zone located in the north-central portion of Nigeria, particularly in the northern Nigerian Basement Complex (Fig. 1). It is bordered by latitudes  $08^{\circ} 30^1 N$  to  $10^{\circ} 30^1 N$  and longitudes  $07^{\circ} 00^1 E$  to  $08^{\circ} 00^1 E$ . The research area also forms part of the Nigerian schist belt and the younger granite province of Northern Nigeria and extends from the south of Kaduna City to the south of Kohawa in the west and from the south of Abaji just around the south-western portion of Robuchi to the south-eastern portion of Onda. It falls within three states in Nigeria and the Federal Capital Territory (Kaduna, Niger, Nasarawa and FCT) (Fig. 2).

### 1.2 Geology and Tectonic Setting of the Study Area

The study area is exclusively Basement Complex and the Basement Complex of Nigeria comprises

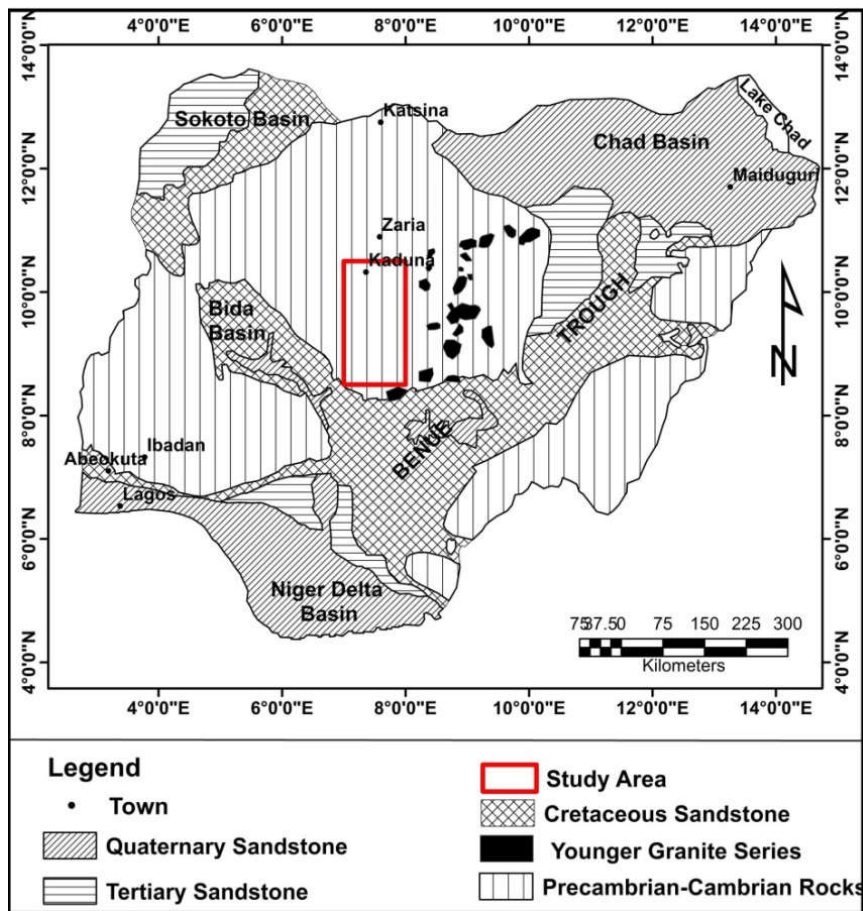


Fig. 1. Generalized geologic map of Nigeria

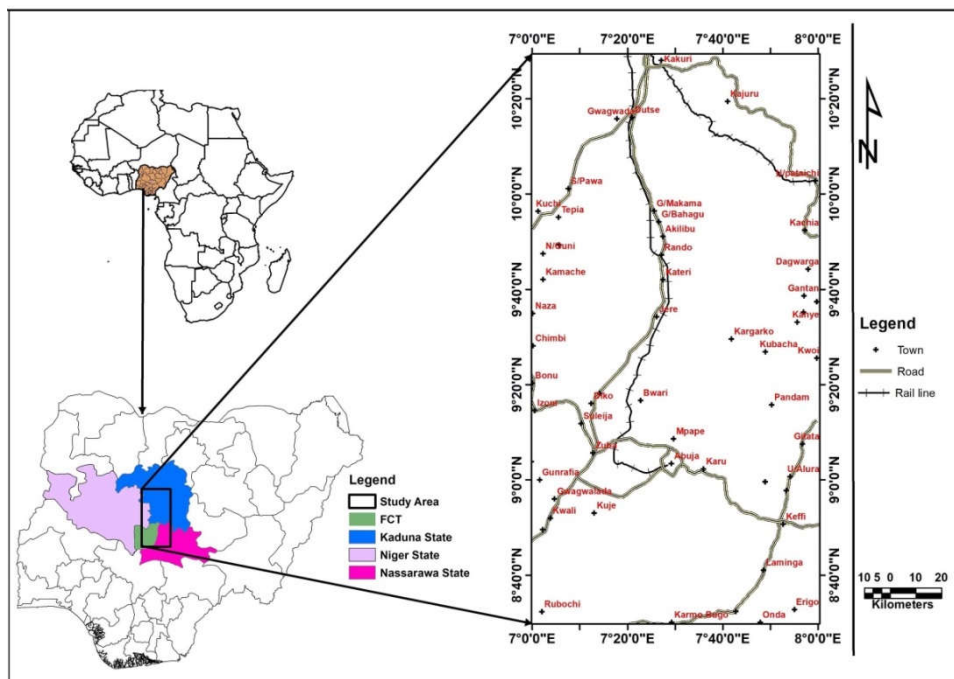
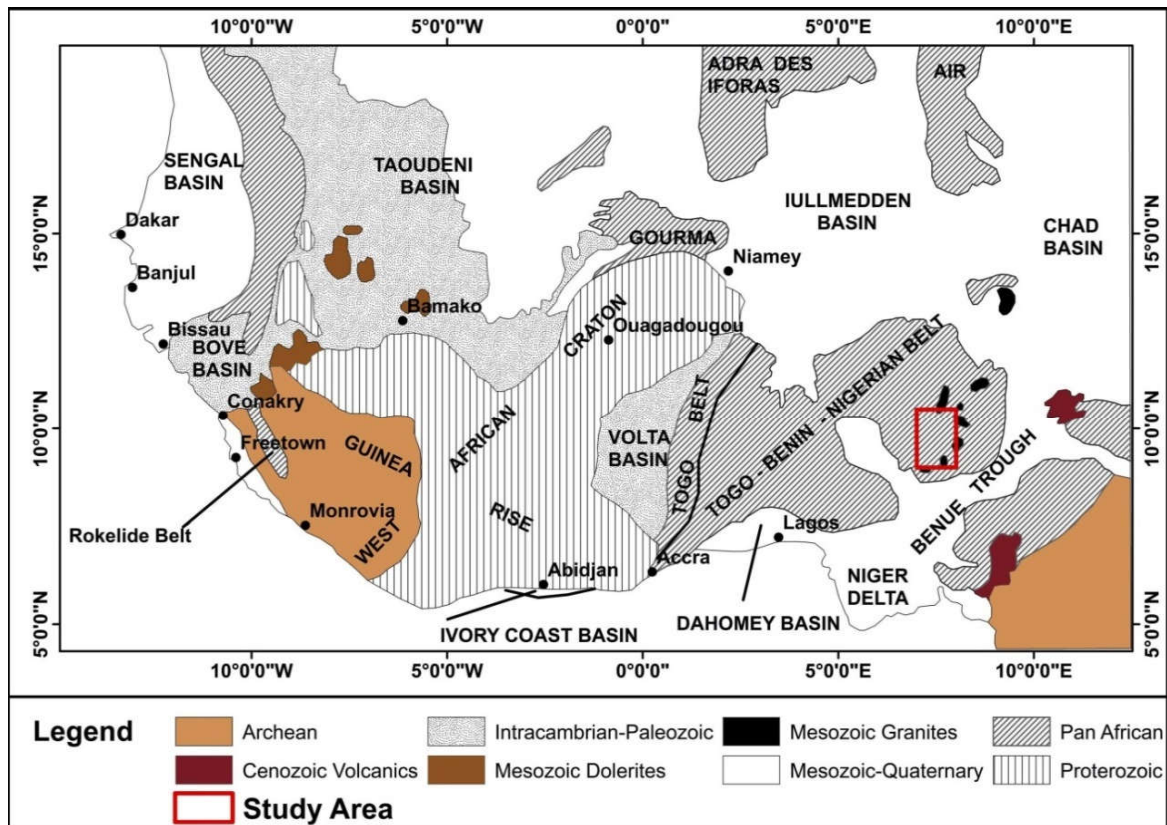


Fig. 2. Location map of the study area



**Fig. 3. Generalized geological map of Nigeria within the framework of the geology of West-Africa (Modified from[33])**

of four major petro-lithological units, namely: Migmatite – Gneiss Complex (MGC), Schist Belt (Metasedimentary and Metavolcanic rocks), Older Granites (Pan African granitoids) and Undeformed Acid and Basic Dykes [26,27]. According to [28 – 32], the Nigerian basement complex, which forms part of the Pan-African mobile belt, is situated between the West African craton; the Congo craton and south of Tuareg shield (Fig. 3) and was deformed by different pre-Cambrian thermo tectonic events, which were accompanied by progressive regional metamorphism. Each of the thermo tectonic events produced characteristic imprints on the basement rocks. However, the Pan-African event was so pervasive that it wipes out most of the structures of the earlier events, leaving only their traces.

Also, as reported by [34,30,31], the structures produced by this widespread event trend commonly N-S to NE-SW whereas those of the other earlier events, including the early part of the widespread Pan-African event trend ENE-WSW, E-W and NW-SE. The thermo tectonic events were also accompanied by the intrusion

of syn-to late-tectonic granites and granodiorites. Common varieties of the granites include porphyritic biotite-and biotite-hornblende granites, as well as non-porphyritic types, commonly non-foliated [28]. These Pan-African granites were termed “Older granites” to distinguish them from the Jurassic (Younger) granites with which they are closely associated in the basement of Northern Nigeria [35]. Recent study of Nigerian basement complex by [36] based on analyses of the Nigeria metallogenic belts, have shown that the stress pattern of the Nigerian landmass has changed appreciably from N-S and NNE-SSW trend to NE-SW and ENE-WSW trend over a period of time from Pan African to Early Cenozoic. These changes have led to the growth of intraplate tensional stresses with the resultant development of intraplate tensional features such as the Sn-Ta pegmatite belt, the Sn-Nb Younger Granite belt and the Pb-Zn Benue Trough in contrast to the N-S compressional plate boundary type related to the continent-continent collision between two entities (the West African craton and the Trans-Saharan mobile belt). The predominant rock type within the research area is Migmatite which

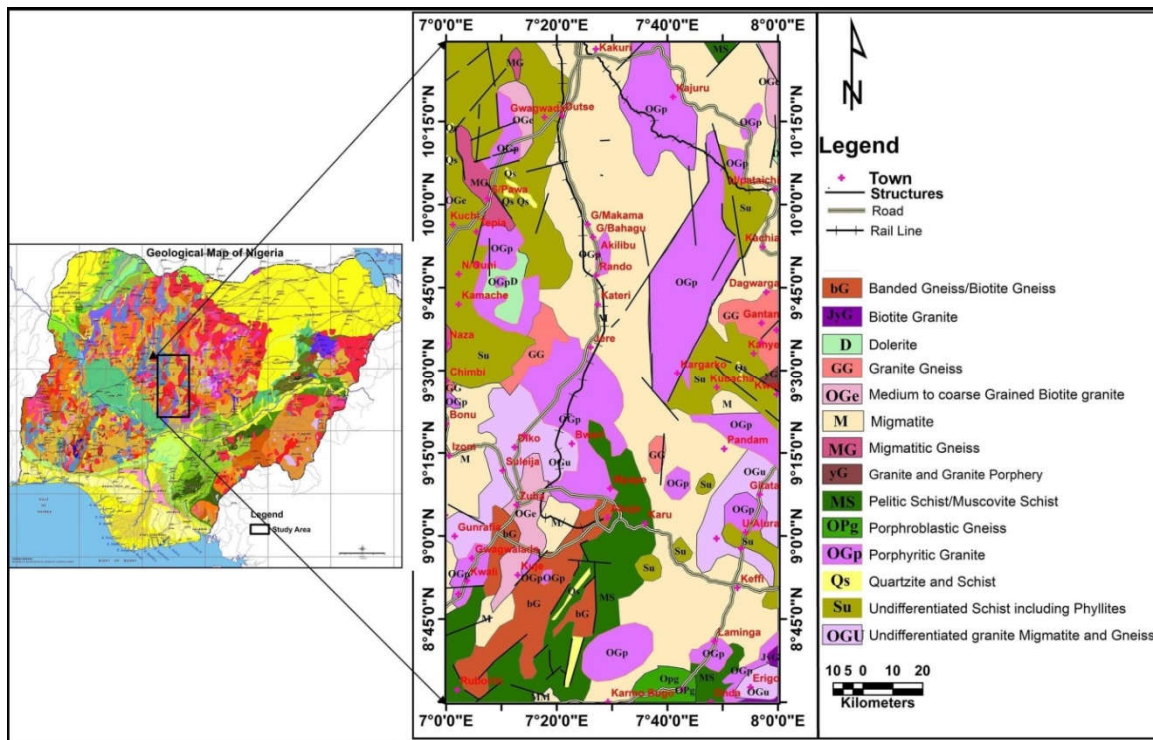


Fig. 4. Geology of the study area

almost covered the entire area with an isolated occurrence of coarse porphyrite Biotite and Hornblend granite, undifferentiated granite, Migmatite and granite gneiss, Biotite Granite, medium to Coarse grained Biotite Granite, Granite and Granite porphyry (Fig. 4).

## 2. MATERIALS AND METHODS

The aeromagnetic data used for this study was acquired from the Nigerian Geological Survey Agency (NGSA) Abuja and consists of sheets (144 Kakuri, 145 Kajuru, 165 Bishini, 166 Kachia, 186 Abuja, 187 Gitata, 207 Kuje and 208 Keffi). Magnetic Data Recording Interval of 0.1 seconds or less (~7m), Sensor Mean Terrain Clearance of 80 meter, Flight Line Spacing, (500) meters, Tie Line Spacing 5000 meters, Flight Line Trend 135 degrees and Tie Line Trend 45 degrees. Also used is shuttle radar topography mission (SRTM) digital elevation model (DEM) covering the study area was taken from united state geologic survey (USGS) web site.

We used software's to conduct our research, Oasis Montaj version 8.3, was used in gridding the magnetic data using the minimum curvature. The total magnetic intensity (TMI) data (Fig. 5a) was reduced to magnetic pole (IGRF of 2005) with magnetic inclination of  $-4.68^\circ$  and

declination of  $-2.01^\circ$  of the center point of the study area (Fig. 5b). This was done to enables the repositioning of magnetic anomalies above their causative source [37 – 39,8,9]. The RTP grid data was upward continued to height of 30km grid which represents the regional field [40,41]. and this regional grid was subtracted from the RTP grid to get the residual grid displayed as a map (Fig. 6a).

According to [11], horizontal gradient magnitude (HGM) or total horizontal derivatives can provide higher resolution and higher precision for wider line spacing. It is essentially important to use while attempting to map linear features such as fault zones and/or dykes from potential field data. The horizontal gradient magnitude of the potential field anomaly was calculated using the Pythagorean sum of the horizontal gradients. For the magnetic field, the Horizontal Gradient Magnitude, (HGM) is calculated as:

$$HGM(x, y) = \sqrt{\left(\frac{\partial T}{\partial x}\right)^2 + \left(\frac{\partial T}{\partial y}\right)^2} \quad (1)$$

where  $\frac{\partial T}{\partial x}$  and  $\frac{\partial T}{\partial y}$  are the horizontal derivatives of the magnetic field in the x and y directions, respectively. This function peaks over contacts/Joints on the assumptions that the

regional magnetic field and magnetic source are vertical among other assumptions. The ridges or maxima of the horizontal derivatives are recognized generally as being good locators of shallow, vertical body edges. This enhancement is complementary to first vertical derivative enhancements. According to [12], the horizontal derivative method will produce apparent contacts that are linear and very continuous and was applied to the aeromagnetic data where major structures were manually mapped out in (Fig. 6b) and displayed in Fig. 7a.

Fig. 7a represent manually delineated structures from HGM in arc Map environment and to produce Fig. 7b, geometry was assigned to the structures (X and Y coordinate of line start and line end). The file was then imported into rockworks version 16 environments that finally created the rose diagram (Fig. 7b) with lineaments (structure) density map (Fig. 7c) produced in arc map environment and exported as jpeg file.

The center for exploration targeting (CET) according to [15, 14], is a suite of algorithms that provide enhancement, lineament detection and Structural complexity analysis functionalities for potential field data. The technique automatically delineates lineaments and can also identifies promising areas of ore deposits within an area of study using total magnetic intensity (TMI) data through outlining regions of convergence and structural element divergence using several statistical steps including textural analysis, lineament detection, and vectorisation (Figs. 8a and 8b). The vectorised structural map produced using Montaj was exported and saved as Esri Shapefile (.shp) where it was imported into arc map version 10.5 and geometry was assigned to the structures (X and Y coordinate of line start and line end). The file was then imported into rockworks version 16 environment that finally created the rose diagram (Fig. 9a). Lineaments (structure) density map (Fig. 9b) was produced in arc map environment and exported as jpeg file.

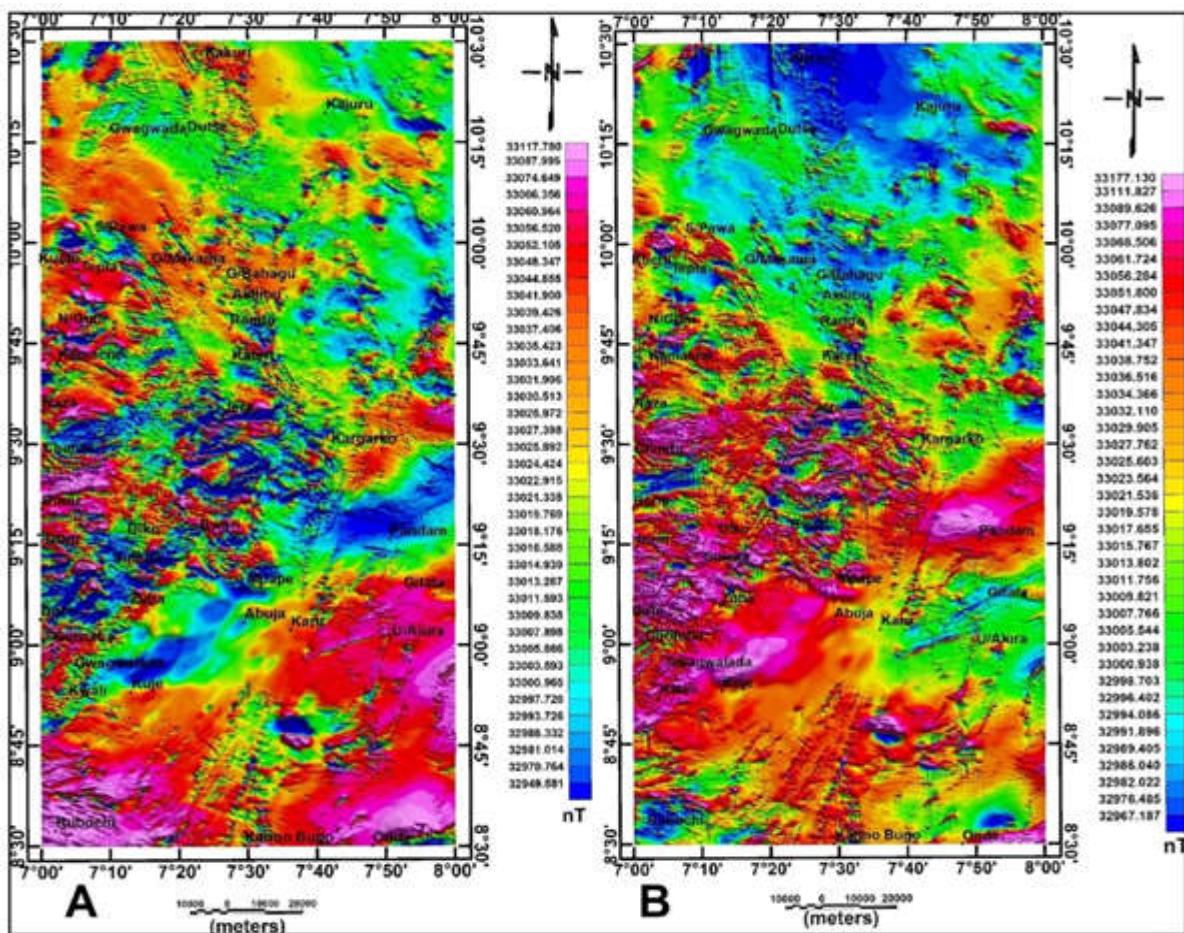


Fig. 5. a. TMI map and b. RTP maps

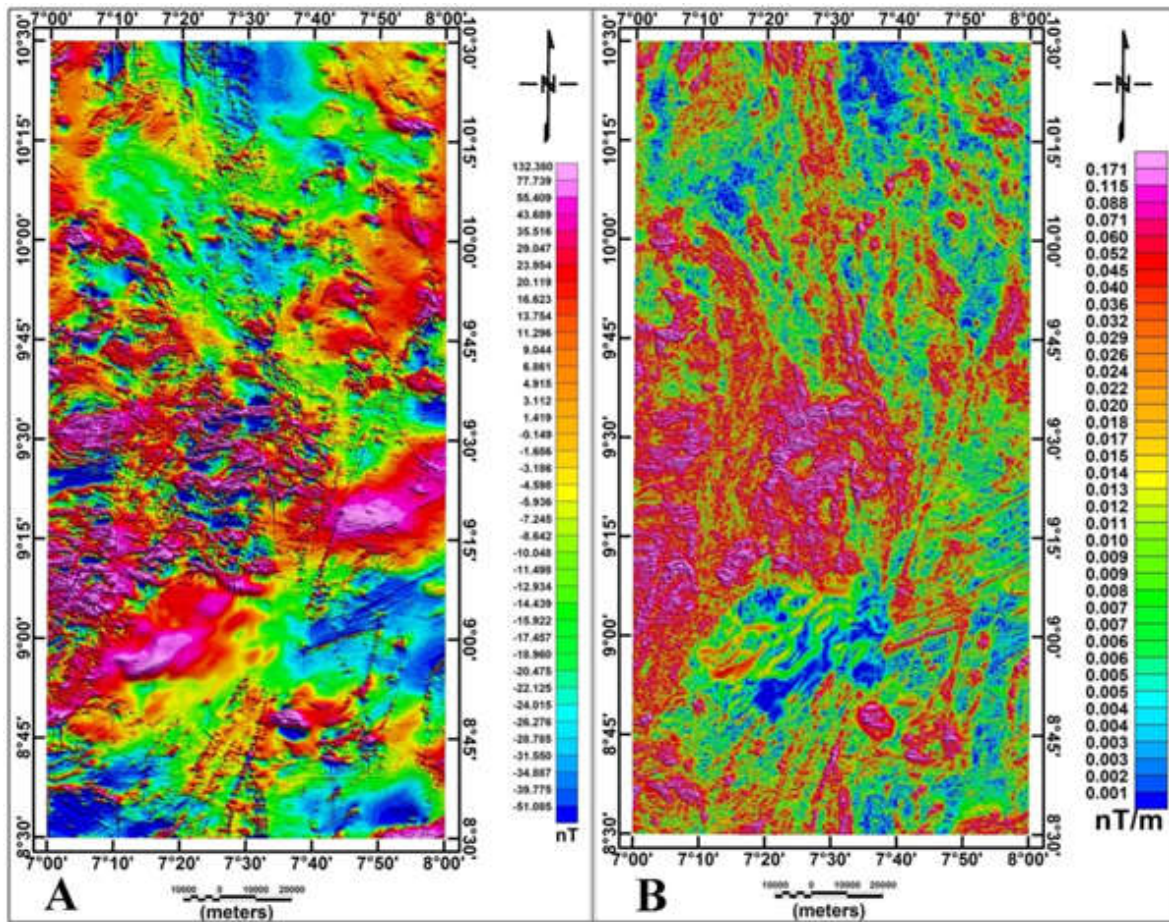


Fig. 6. a. RMI map and b. Horizontal Gradient Magnitude map

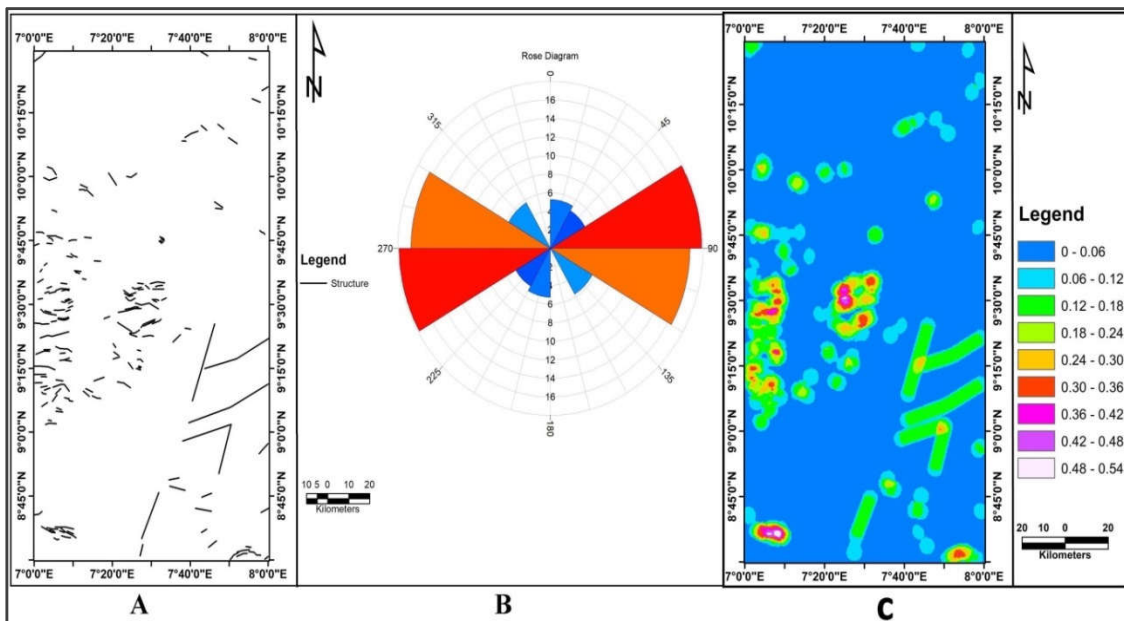


Fig. 7. a. Structural map from HGM b. Rose diagram and c. structural density map

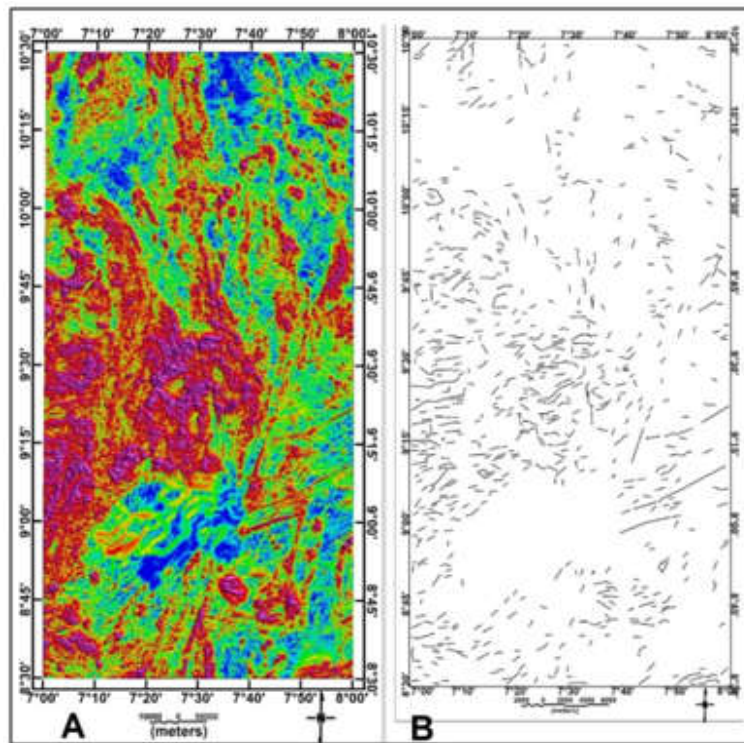


Fig. 8. a. Standard deviation and b. Vectorised structural map

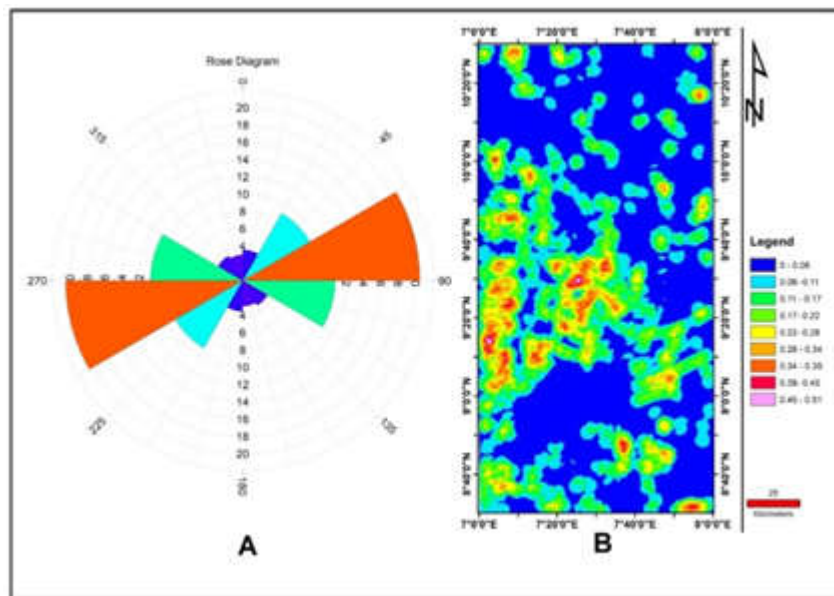


Fig. 9. a. Rose diagram and b. lineament density map

The standard Euler Deconvolution method was applied to the RTP grid data of the study area, using structure index 0, 1, 2 and 3 to delineate the depth and location of the basement rock contact and/or faults with dykes (N= 0 for contacts, 1 for sill / dyke / fault, 2 for pipe / horizontal bodies, and 3 for spherical bodies). The obtained Euler solution maps Fig. 10 (a and b) and Fig. 11 (a and b).

The 3D Euler deconvolution has proven to be a robust interpretation tool in the interpretation of magnetic data because it requires little prior information on the geometry of magnetic sources. Another advantage of this technique is that it requires no knowledge of the vector magnetization [42, 16], it can therefore be applied to regions where the causative magnetic source is hidden and where the geology of the location

is not well known. Largely, this technique has been used extensively to outline the edges and shapes of sources from potential field image map[43 – 46]. 3D Euler deconvolution extracts data from grids using the homogeneity relationship shown by ([41]). This relationship can be written in the following form:

$$(x - x_0) \frac{\delta T}{\delta x} + (y - y_0) \frac{\delta T}{\delta y} + (z - z_0) \frac{\delta T}{\delta z} = N(B - T) \quad (2)$$

Where  $(x_0, y_0, z_0)$  is the position of a magnetic source whose total field  $T$  is detected at  $(x, y, z)$ .  $B$  is the regional field value, and the degree of homogeneity interpreted as the structural index (SI) which is a measure of the rate of change at field distance is represented by  $N$ , and this structural index was chosen based on prior knowledge of the source geometry. To correlate Euler deconvolution and HGM, the Euler solution for structural index of one (SI=1) was plotted on the HGM map in Oasis Montaj environment (Fig. 12a).

The source parameter imaging (Fig. 12b) has been employed to determine the depth to the

magnetic source within the study area. [17 – 19] developed the source parameter imaging (SPI) technique, based on the complex analytic signal, which computes source parameters from gridded magnetic data. The technique is sometimes referred to as the local wavenumber method. The local wavenumber has maxima located over isolated contacts, and depths can be estimated without assumptions about the thickness of the source bodies[47]. Based on[17], the basics are that for vertical contacts, the peaks of the local wavenumber define the inverse of depth. The Source Parameter Imaging (SPI) method calculates source parameters from gridded magnetic data. SPI is a technique based on the extension of complex AS to estimate magnetic depths; it is also known as local wavenumber. The original SPI method works for two models: a 2-D sloping contact or a 2-D dipping thin-sheet. For the magnetic field  $f$ , the local wavenumber is given by equation 6:

$$k = \frac{\frac{\partial^2 f \partial f}{\partial x \partial z \partial x} \frac{\partial^2 f \partial f}{\partial x^2 \partial z}}{\left(\frac{\partial f}{\partial x}\right)^2 + \left(\frac{\partial f}{\partial z}\right)^2} \quad (3)$$

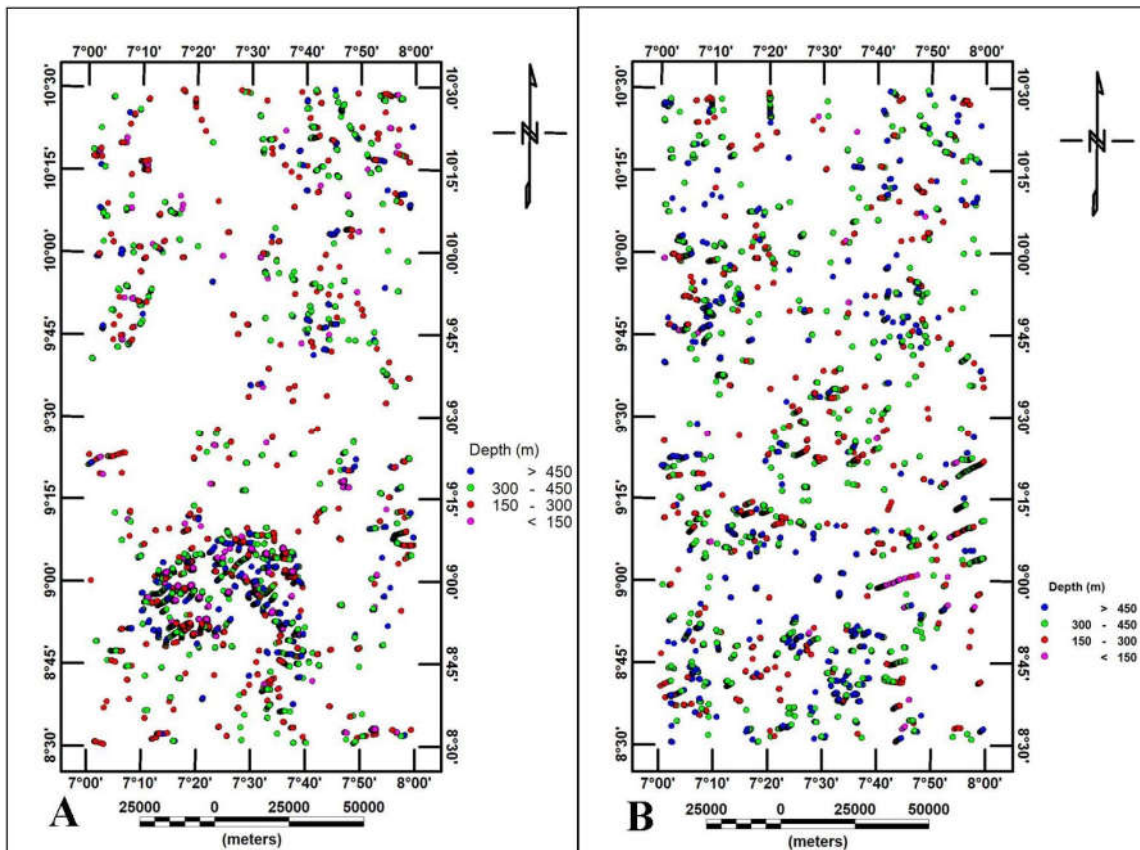


Fig. 10. a. Euler deconvolution SI = 0 for contacts and b. Euler deconvolution SI = 1 for sill/dyke/fault

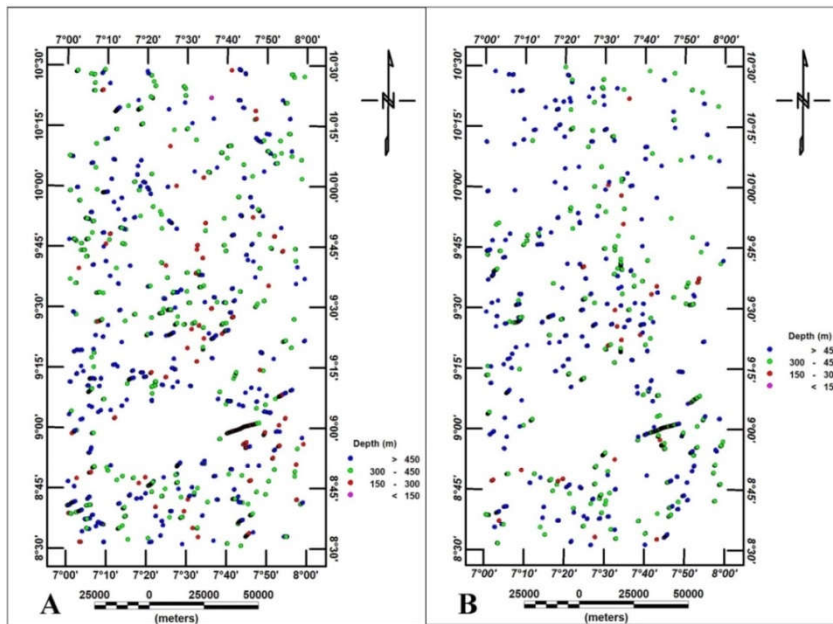


Fig. 11. a. Euler deconvolution, SI=2 for pipes and horizontal bodies' b. Euler deconvolution, SI=3 for spherical bodies

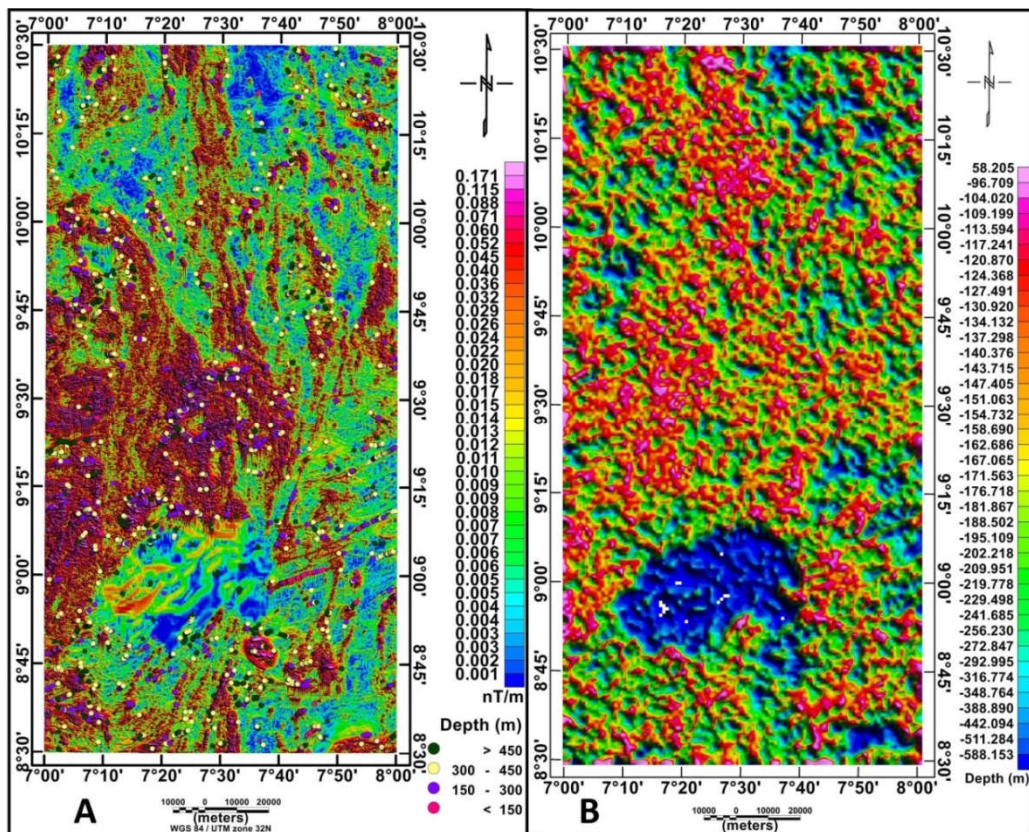


Fig. 12. a. HGM Map with Euler Solution (SI = 1) b. Depth to Magnetic Source Map (SPI)

For the dipping contact, the maxima of  $k$  are located directly over the isolated contact edges and are independent of the magnetic inclination, declination, dip,

strike and any remnant magnetization. The depth is estimated at the source edge from the reciprocal of the local wavenumber i.e

$$Depth_{x=0} = \frac{1}{k_{max}} \quad (4)$$

Where  $k_{max}$  is the peak value of the local wavenumber K over the step source [17].

### 3. RESULTS AND DISCUSSION

#### 3.1 Qualitative Interpretation

According to [48], the qualitative interpretation of aeromagnetic data directly illustrates geological information by looking at an aeromagnetic map without any calculations. A visual inspection of magnetic maps can be fruitful for preliminary interpretation [49]. Visual studies of total aeromagnetic intensity (TMI) and total magnetic intensity reduced to the pole (RTP) maps (Fig. 5a and 5b) and the residual aeromagnetic intensity map (Fig. 6a) of the central part of Nigeria revealed variations in the magnetic field intensity throughout the area and such variation is a function of the rock types, differences in the sizes, depths, and magnetic susceptibilities of the underlying rocks. The TMI map (Fig. 5a) and the RTP map (Fig. 5b) emphasizes the magnetic intensities and the wavelength/frequencies of the anomalies within the area that is comprised of both regional and local sources. Most of the anomalies trend in the NE–SW direction, while others trend in the E–W especially within the central portion of the map to the west and NW–SE directions.

The alternating occurrence of magnetic high and lows within TMI and RTP maps could be attributed to faults/highly fractured nature of the area as oxidation in fractured zones during weathering processes commonly leads to the destruction of magnetite which often allows such zones to be picked out on anomaly maps as narrow zones with markedly less magnetic variation than in the surrounding rocks [50]. Also, the effect of metasomatic alteration of magnetite and /or hydrous Fe-oxide developed in fractures can lead to a decrease in the magnetic susceptibility of the host rocks [51].

Magnetic intensity values vary from 32949.581 nT minimum to 33117.780 nT maximum on the TMI map, magnetic high is observed around the southern portion of the map and within the central portion. The positions of the magnetic lows and highs have now changed as areas showing magnetic low on the TMI map are now showing high on the RTP map (Fig. 6b). Also, RTP map has magnetic intensities that vary from 32967.187 nT minimum to 33177.130 nT

maximum. Within the central portion of the RTP map to the western end, the magnetic highs within these areas could be attributed to basic magmatic intrusions.

The residual magnetic intensity map (Fig. 7a) has magnetic intensity values ranging from -51.085 nT low to 132.380 nT high. The short-wavelength (high-frequency signatures) occurs within the central portion of the map and span through the end of the map in the west. The long-wavelength (low-frequency signatures) is predominant within the south-west, south-east and northern part of the map.

#### 3.2 Quantitative Interpretation

##### 3.2.1 Structural lineament trends

The horizontal gradient magnitude (HGM) map (Fig. 6b) has produced maximum ridges over the edges of contacts or faults within the study area. The horizontal gradient magnitude map peaks locations and directions of maxima within the study area that is mapped out manually using black lines as displayed in Fig. 7a. Inspection of HGM structural map (Fig. 7a) reveals structures that were statistically analysed (Fig. 7b) to be trending majorly in ENE-WNW and WNW-ENE directions with minor NE-SW, NNE-SSW and NW-SE trends. While lineament density analysis map (Fig. 7c) of the manual structures delineated using the HGM showed the central portion of the map to be very dense with structures which could be prospective for mineralization.

The center for exploration targeting, starting with the standard deviation map of the study area (Fig. 8a) shows the area in (blue coloration) which indicated very little variation in the magnetic intensity data of the study area. Areas (Red to Pinkish coloration) with moderate to high variation in magnetic intensity within the study area are concentrated within the central portion of the map and span toward the west to the end of the map are attributed to shallow or exposed magnetic source. Also, the vectorised structural map (Fig. 8b) reveals the central portion of the study area to be highly deformed and dissected by many tectonic trends. Fig. 9a depict the lineaments that were automatically extracted to be trending also just like the manually extracted lineament rose diagram (Fig. 7b) in ENE-WSW, WNW-ESE, NE-SW, NW-SE, NNE-SSW and NNW-SSE directions. Statistical trend analysis of the structures using the rose diagram (Fig. 9a) showed that the largest petal which is 40.60 % of total delineated lineaments; represent lineaments

trending in the East-North-East to West-South-West (ENE-WSW) direction. Fig. 9a also indicates that out of delineated lineaments plotted, 17.80% represented petal striking in the northeast-southwest (NE-SW) direction with 21.30% of the structures striking West-South-West to East-North-East (WNW-ESE) and another 6.90 % trending in the northwest-southeast (NW-SE) direction. Also, the North-North-East to South-South-West (NNE-SSW) trending structures accounted for 7.5 % while North-North-West to South-South-East (NNW-SSE) trending structures accounted for 5.90 % of the total structures within the study area. Dominant structural trend base on the analysis is the East-North-East to West-South-West (ENE-WSW) followed by the structures trending in West-South-West to East-North-East (WNW-ESE) direction.

Fig. 10(a and b) and Fig. 11(a and b) show 3D Euler depth solutions for location of the basement rock contact and/or faults with dykes (N= 0 for contacts, 1 for sill / dyke / fault, 2 for pipe / horizontal bodies, and 3 for spherical bodies) that were grouped into four groups, those below 150 m, 150 m to 300 m, those between 300 m to 450 m and those above 450 m respectively and in the four maps, contact and/or faults with dykes (N= 0 for contacts, 1 for sill / dyke / fault, 2 for pipe / horizontal bodies, and 3 for spherical bodies) between 300 m – 400 m depth dominates. Also, when Euler solutions with structural index of one (SI=1) were plotted on the HGM map (Fig. 12a), the resultant map has shown that the two method can contribute in delineating the general structural framework of the study area.

The SPI map for the study area Fig. 12b displays depth to magnetic sources across the study area. The white portions on the map signify areas, where the derivative used for the estimation of the local wavenumber is so small that the SPI structural index cannot be estimated reliably. Depths to magnetic source bodies within the study area vary from 58.205 m to 588.153 m. Some deep zones (588.153 m) to source bodies were observed in various parts of the map. The deep zones are more pronounced in the north-western and north-eastern parts of the study area and the southern part of the study area. Depth from SPI can be correlated with depth obtained from 3D Euler deconvolution method.

#### 4. CONCLUSIONS

Base on the results from the structural analysis of the aeromagnetic data, we conclude that, the

study area has been affected and dissected by two predominant sets of structures that trend ENE-WSW and WNW-ENE with minor NE-SW, NW-SE, NNE-SSW and NNW-SSE. The occurrences of these structures are predominant within 300 m to 450 m depth as obtained from 3D Euler deconvolution. These depths correlate with depth obtain from source parameter imaging which shows that the two methods complement each other in depth to magnetic source estimations.

#### COMPETING INTERESTS

Authors have declared that no competing interests exist.

#### REFERENCES

1. Kearey P, Brook SM, Hill I. Introduction to geophysical exploration. 3rd Edition. Blackwell Scientific Publication, Oxford. 2002;156-159.
2. Clark D. Magnetic properties of rocks and minerals. *AGSO Journal of Australian Geology and Geophysics*. 1997;17(2):83-103.
3. Murray AS, LM Tracey. Best practice in gravity surveying, Geoscience Australia; 2004. Available:<http://www.ga.gov.au/pdf/RR0027.pdf>
4. Grauch VJS, Milligan PS. Mapping intrabasinal faults from high resolution aeromagnetic data: The Leading Edge. 1998;17(1):53-55.
5. Gunn P. Airborne Magnetic and Radiometric Survey. *AGSO Journal of Australian Geology and Geophysics*. 1997;17(2):216.
6. Reeves CV, Reford SW, Milligan PR. Airborne Geophysics: Old methods, new images in Gubbins, A.G.(ED). *Proceedings of Exploration 97, Fourth Decennial International Conference on Mineral Exploration*. 1997;13-30.
7. Reeves CV. Continental scale and global geophysical anomaly mapping: *ITC Journal*. 1998;2: 91-98.
8. Milligan PR, Gunn PJ. Enhancement and presentation of airborne geophysical data. *AGSO Journal of Australian Geology and Geophysics*. 1997;17(2):64–774.
9. Baranov V. A new method of interpretation of aeromagnetic maps: Pseudogravimetric anomalies. *Geophysics*. 1957;22:259-283.

10. Bhattacharyya BK. Two-dimensional harmonic analysis as a tool for magnetic interpretation. *Geophysics*. 1965;30:829-857
11. Hogg S. GT-Gradient tensor gridding Available:<http://www.shageophysics.com/>
12. Phillips JD. Locating Magnetic Contacts; A Comparison of the Horizontal Gradient, Analytic Signal and Local Wavenumber Methods: Society of Exploration Geophysicists, Abstracts with Programs, Calgary. 2000;402–405.
13. Grauch VSJ, Cordell L. Limitations of determining density or magnetic boundaries from the horizontal gradient of gravity or pseudogravity data. Short note, *Geophysics*. 1987;52(1):118–121.
14. Holden EJ, Dentith M, Kovesi P. Towards the automatic analysis of regional aeromagnetic data to identify regions prospective for gold deposits”, *Computers & Geosciences*. 2008;34(11): 1505–1513.
15. Core D, Buckingham A, Belfield S. Detailed structural analysis of magnetic data done quickly and objectively, *SGEG Newsletter*; 2009.
16. Reid AB, Allsop JM, Granser H, Millet AJ, Somerton IW. Magnetic interpretation in three dimensions using Euler deconvolution. *Geophysics*. 1997;55:80-91.
17. Thurston JB, Smith RS. Automatic conversion of magnetic data to depth, dip, and susceptibility contrast using the SPI method. *Geophysics*. 1997;62(3):807–813.
18. Thurston J, Guillon JC, Smith R. Model-independent depth estimation with the SPITM method: 69<sup>th</sup>Annual International Meeting, SEG, Expanded Abstracts. 1999;403–406.
19. Thurston JB, Smith RS, Guillon JC. A multi-model method for depth estimation from magnetic data. *Geophysics*. 2002;67(2):555–561.
20. Daniel E, Jimoh R, Lawal K. Delineation of Gold Mineral Potential Zone Using High Resolution Aeromagnetic Data Over Part of Kano State, Nigeria, *J Geol Geophys*. 2019;8:464. DOI: 10.35248/2381-8719.464
21. Andrew J, Alkali A, Salako KA, EE Udensi. Delineating Mineralisation Zones within the Keffi- Abuja Area Using Aeromagnetic Data. *Journal of Geography, Environment and Earth Science International*; 2018. DOI: 10.9734/JGEEESI/2018/37052
22. Balogun OB. Tectonic and structural analysis of the Migmatite–Gneiss–Quartzite complex of Ilorin area from aeromagnetic data *NRIAG Journal of Astronomy and Geophysics*; 2019. Available:<https://doi.org/10.1080/20909977.2019.1615795>
23. Okwokwo, O. I., Adetona AA, Adewumi T, Adediran SO. Interpretation of high resolution aeromagnetic data to determine sedimentary thickness over part of Bida Basin, North Central Nigeria: *Journal of Geology and Mining Research*. 2018;10(6):72-80. DOI: 10.5897/JGMR2018.0293
24. Salako KA. Depth to Basement Determination Using Source Parameter Imaging (SPI) of Aeromagnetic Data: An Application to Upper Benue Trough and Borno Basin, Northeast, Nigeria. *Academic Research International*. 2014;5(3). ISSN: 2223-9944, eISSN: 2223-9553
25. Megwara JU, Udensi EE. Structural Analysis Using Aeromagnetic Data: Case Study of Parts of Southern Bida Basin, Nigeria and the Surrounding Basement Rocks. *Earth Science Research*. 2014;3(2). DOI: 10.5539/esr.v3n2p27
26. Obaje NG. *Geology and Mineral Resources of Nigeria*, Berlin: Springer-Verlag, Heidelberg. 2009;1-221.
27. NGSA. *Geology and Structural Lineament Map of Nigeria*; 2006.
28. McCurry P. Pan-African Orogeny in Northern Nigeria. *Geol. Soc. Am. Bull*. 1971a;82:3251-3262.
29. Rahaman MA. Progressive polyphase metamorphism in pelitic schists around Aiyetoro, Oyo State, Nigeria. *J. Min. Geol*. 1976a;13:33-44.
30. Grant NK. Structural distinction between metasedimentary cover and underlying basement in 600 M.Y. old Pan-African domain. *Geol. Soc. Am. Bull*. 1678;89:50-58.
31. Ekweme BN. Structural orientation and precambrian deformational episode of Uwet area, Oban Massif, S. E. Nigeria. *Precambrian Res*. 1987;34:269-289.
32. Ekwueme BN. Structural features of Obudu Plateau, Bamenda Massif, Eastern Nigeria: Preliminary interpretation. *J. Min. Geol*. 1994;30(1):45-59.
33. Wright JB. *Geology and mineral resources of West Africa*. George Allen and Unwin, London. 1985;187.

34. McCurry P. Plate tectonics and the Pan-African Orogeny in Nigeria. *Nature*. 1971b;229:154-155.
35. Falconer JD. *The Geology and Geography of Northern Nigeria*. Macmillan, London; 1911.
36. Haruna IV. Review of the Basement Geology and Mineral Belts of Nigeria. *Journal of Applied Geology and Geophysics (IOSR-JAGG)* e-ISSN: 2321-0990, p-ISSN: 2321-0982. 2017;5 (1)Ver. I:37-45
37. Lou Y, Xue DJ, Wang M. Reduction to the Pole at the Geomagnetic Equator. *Chinese Journal of Geophysics*. 2010;53(6):1082-1089.
38. Li X. Magnetic reduction-to-the-pole at low latitudes; 2008.
39. Yaoguo L, Douglas WO. Stable reduction to the pole at the magnetic equator *Geophysics*. 2001;66(2):571-578.
40. Reynolds JM. *An introduction to Applied and Environmental Geophysics*, John Wiley and Ltd. Bans Lane, Chichester. 1997;124-13.
41. Telford WM, Geldart LP, Sherriff RE, Keys DA. *Applied geophysics*. Cambridge: Cambridge University Press. 1990;860.
42. Thompson DT. EULDPH: a new technique for making computer-assisted depth estimates from magnetic data. *Geophysics*. 1982;47:31-37.
43. Salawu NB, Olatunji S, Orosun MM, Abdulraheem TY. Geophysical inversion of geologic structures of Oyo Metropolis, Southwestern Nigeria from airborne magnetic data. *Geomech Geophys Geo-energy Geo-Resour*. 2019;5:143-157.
44. El-Akrab AM, Khalifa MO, Fraihy WD. Aeromagnetic data interpretation for delineation of the subsurface structures of the area east Qena provenance, Central Eastern Desert, Egypt; 2016. [ISSN: 2394-5710]
45. Amar N, Khattach D, Azdimousa A, Chourak M, Jabaloy A, Manar A, Amar M. Structure and peridotite of Gibraltar arc southern bloc: gravimetric and aeromagnetic evidences *Arabian Journal of Geosciences*; 2015. DOI: 10.1007/s12517-015-1879-3
46. Saada SA. Edge detection and depth estimation from magnetic data of wadi Araba, eastern desert- Egypt. *IOSR Journal of Applied Geology and Geophysics (IOSR-JAGG)*. 2015;3(6);33-45 e-ISSN: 2321-0990, p-ISSN: 2321-0982
47. Smith RS, JB Thurston, TF Dai, IN MacLeod. iSPI — the improved source parameter imaging method: *Geophysical Prospecting*. 1998;46:141-151.
48. Grant FS, West GF. *Interpretation theory in Applied Geophysics*. New York: McGraw-Hill; 1965.
49. Telford WM, Geldart LP, Sheriff RE. *Applied Geophysics*, 2nd Edition, Cambridge University Press, USA. 1998;770.
50. Reeves C. *Aeromagnetic surveys, principle practice and interpretation*. Geosoft E-Publication; 2005. Available:www.geosoft.com/media/uploads/resources/technical/aeromagnetic\_survey\_Reeves.pdf
51. Isles DD, Rankin LR. *Geological interpretation and structural analysis of aeromagnetic data*. TGT Consulting/Geointerp Unpublished workshop manual Fugro Gravity and Magnetic Services. Houston, USA: Fugro; 2011

© 2020 Tawey et al.; This is an Open Access article distributed under the terms of the Creative Commons Attribution License (<http://creativecommons.org/licenses/by/4.0>), which permits unrestricted use, distribution, and reproduction in any medium, provided the original work is properly cited.

*Peer-review history:*  
 The peer review history for this paper can be accessed here:  
<http://www.sdiarticle4.com/review-history/60263>